Macromolecules

pubs.acs.org/Macromolecules Article

Stability of Diverse Dodecagonal Quasicrystals in T-Shaped Liquid Crystalline Molecules

Xin Wang, An-Chang Shi,* Pingwen Zhang,* and Kai Jiang*

Cite This: *Macromolecules* 2025, 58, 5229−5239 Read Online

ACCESS | Metrics & More | Article Recommendations | Supporting Information

ABSTRACT: Quasicrystals are intriguing ordered structures characterized by quasiperiodic translational and noncrystallographic rotational symmetry. The tiling of different geometric units such as triangles and squares in two-dimensional space can result in a great variety of quasicrystals that could be realized by the self-assembly of liquid crystalline molecules. In this study, we introduce three self-similar dodecagonal tilings, including a novel diamond−square−triangle pattern, composed of triangular and quadrangular tiles, and examine their thermodynamic stability by using the self-consistent field theory applied to T-shaped liquid crystalline molecules. Specifically, we detail the inflation rules for the construction of these dodecagonal tilings, analyze their self-similarity, and show that these tilings can be viewed as projections of higher-dimensional periodic lattice points with projection windows. Using these dodecagonal tilings as initial configurations of the SCFT results in solutions corresponding to quasicrystals that could form from T-shaped liquid crystalline molecules. The relative stability of these aperiodic phases is analyzed to obtain design rules that could stabilize quasicrystals. Meanwhile, we provide a criterion for distinguishing three dodecagonal quasicrystals and their approximants by analyzing their diffraction peaks. These findings shed new light on the discovery of new quasicrystals in soft materials.

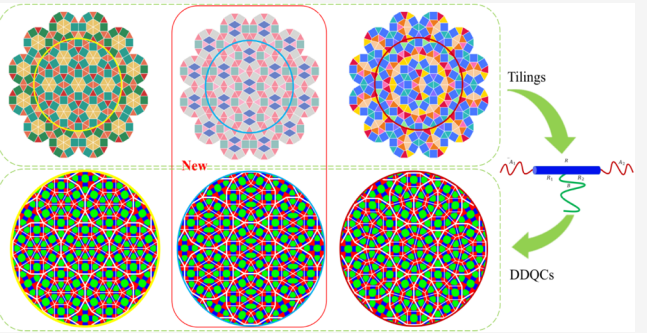

INTRODUCTION

Quasicrystals (QCs) are fascinating structures that possess quasiperiodic translational and noncrystallographic rotational symmetry. The discovery of QCs in Al−Mn alloys in 1984 was a breakthrough that changed the perception of crystalline order.[1] Since then, thousands of metallic alloys have been found to exhibit quasicrystalline order.[2] Furthermore, QCs have been observed in a wide range of soft materials, including block copolymers,[3−5] liquid crystalline molecules,[6−8] nanoparticles,[9] colloidal particles,[10] mesoporous silica,[11] silicon bilayers,[12] and DNA motifs.[13,14] It is interesting to note that the majority of soft QCs adopt 12-fold rotational symmetry, while only a few of them are with 10- and 18-fold rotational symmetries.[10,15,16] These soft QCs are quasiperiodic in a plane while homogeneous or periodic normal to the plane. Here, "homogeneous" refers to the structure exhibiting a columnar form in the normal direction, similar to the columnar quasicrystals described in the literature.[8] Therefore, they are regarded as two-dimensional (2D) QCs. The patterns of 2D dodecagonal QCs (DDQCs) observed experimentally are mainly square−triangle (ST)[5,17,18], and quadrangle−square−triangle (QST) tilings.[8,19] Only the ST tiling has been considered theoretically.[4] Despite great progress made over the years, the discovery and stability analysis of diverse DDQCs remain relatively unexplored.

In general, the study of thermodynamic stability of ordered phases requires a specific physiochemical system that exhibits the desirable phase behavior and a theoretical framework that allows accurate calculation of the free energies of different phases. Therefore, systems capable of self-assembling into polygonal structures are of great interest for studying soft QCs. For the purpose of studying the emergence and relative stability of various DDQCs that could be constructed from polygonal tiles, a suitable soft matter system is the T-shaped liquid crystalline molecules (TLCMs) shown in Figure 3. Extensive experimental studies on this class of molecules have demonstrated their self-assembly into rich polygonal structures, such as triangle, dual-pentagon, diamond, square, pentagon, hexagon, octagon, decagon,[20−31] and even DDQCs.[8] The rich phase behaviors of the TLCMs make them an ideal platform for studying the relative stability of diverse DDQCs in soft materials.

Received: September 29, 2024
Revised: April 21, 2025
Accepted: April 29, 2025
Published: May 8, 2025

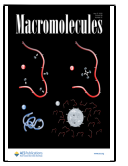

https://doi.org/10.1021/acs.macromol.4c02380
Macromolecules 2025, 58, 5229−5239

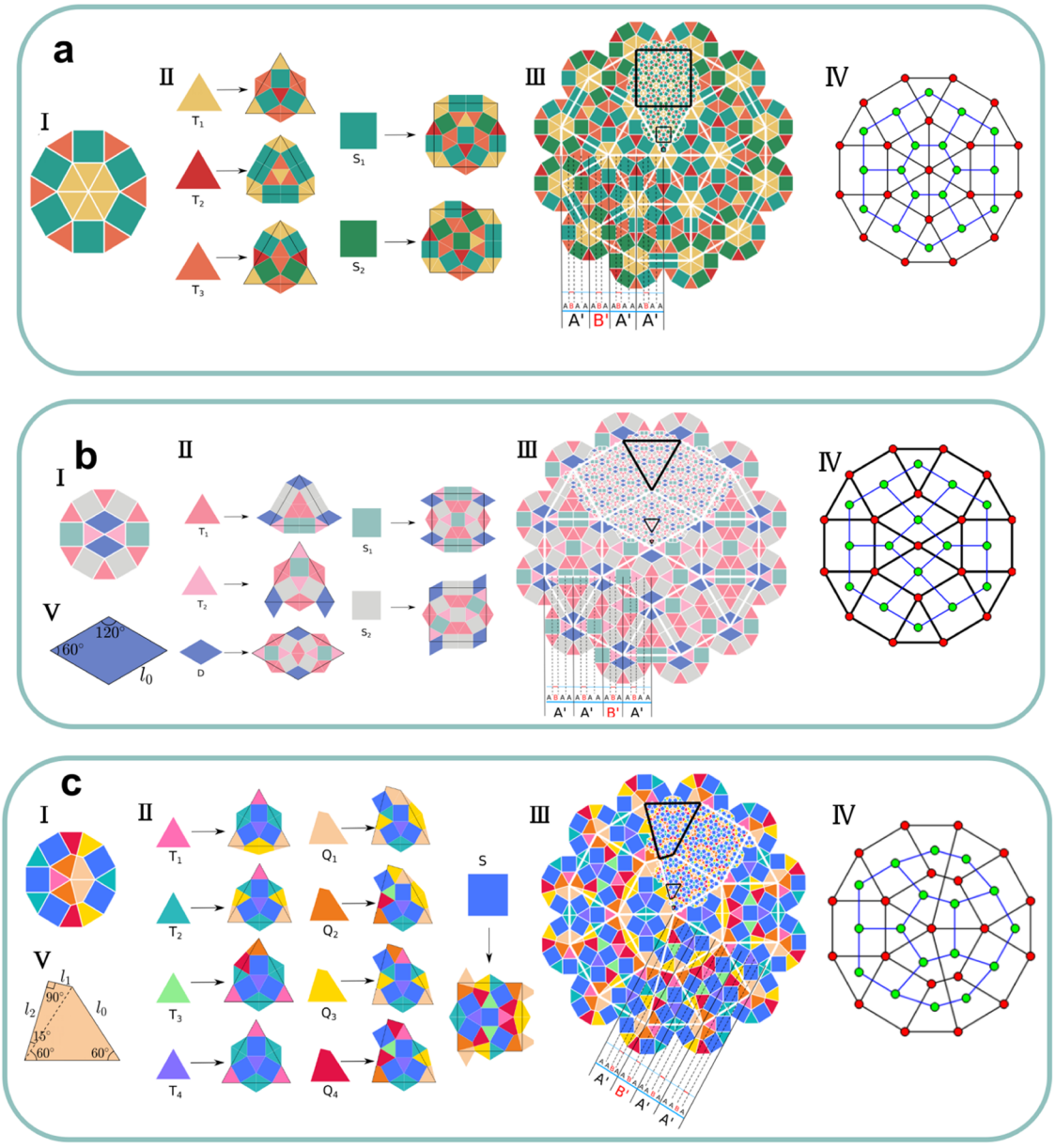

Figure 1. Three dodecagonal aperiodic tilings are noticed: (a) square−triangle (ST) tiling, (b) diamond−square−triangle (DST) tiling, (c) quadrangle−square−triangle (QST) tiling, (I) fundamental dodecagon, (II) inflation rules of prototiles, and (III) second-generation tilings of (I). In the second-generation tilings, parallel line sets show that vertex spacings ("letters") *A* and *B* of the given generations construct aperiodic sequences by substituting $\{A^3B \rightarrow A', A^2B \rightarrow B'\}$. The black-outlined parts in the third-generation pattern are self-similar. (IV) Schematic tilings of fundamental dodecagons. The green vertices form dual tilings of these dodecagonal tilings (red vertices). (V) Diamond and quadrangle tiles.

On the theoretical front, several frameworks have been proposed to study the stability of QCs. One widely used class of theories depends on the construction of multilength-scale free energy functionals, such as phenomenological Landau-type theories[32,33] and density functional theories.[34] These models are suitable for investigating generic features of QCs and their phase transitions.[35−37] However, these theories usually start from certain hypothesized multilength-scale correlation potentials, making it difficult to connect the theory with concrete physical systems. Another widely used class of theories is the self-consistent field theory (SCFT), which is a powerful framework for accurately describing the self-assembly behavior of inhomogeneous soft materials, particularly polymers and liquid crystal polymers.[38−41] Over the past decades, the SCFT has been successfully applied to studying the phase behaviors of various flexible and semiflexible polymer systems.[42−45] The success of SCFT makes it a useful framework to study the phase behaviors of complex molecules, such as the TLCMs.

In this work, we study the emergence and relative stability of various two-dimensional QCs in TLCMs by using dodecagonal aperiodic tilings as initial candidate phases of the SCFT. Starting from the aperiodic tiling theory, we analyze the existing dodecagonal ST tiling and QST tiling and then propose a novel dodecagonal diamond−square−triangle (DST) tiling. The respective inflation rules of these structures are presented in detail. Meanwhile, a cut-and-project method is used to analyze these tilings and obtain the corresponding projection windows. In the second step of the study, we develop an SCFT framework for TLCMs, utilizing the Maier−

https://doi.org/10.1021/acs.macromol.4c02380
Macromolecules 2025, 58, 5229−5239

Saupe interaction to represent the orientational interaction of rigid rods. Using the constructed dodecagonal tilings as initial structures, we obtain solutions of the SCFT equations corresponding to three DDQCs as well as other candidate phases. The free energies of these phases are then used to determine their relative stability. Finally, we introduce random DDQCs and obtain SCFT solutions of all ideal and random DDQCs in TLCMs, then perform energy analysis to predict possible ways for stabilizing DDQCs. For three DDQCs and their approximants, we provide a criterion for distinguishing them by analyzing their diffraction peaks.

DODECAGONAL APERIODIC TILINGS

The main task of the SCFT study is to obtain solutions of the SCFT equations. Almost all of the numerical methods of solving the SCFT equations are iterative in nature; thus, the solutions depend crucially on the initial configurations. Over the years, various methods have been developed to construct initial configurations, leading to solutions corresponding to various periodically ordered phases.[46] However, there have been few studies of the construction of initial configurations for QCs. We propose using aperiodic tilings to construct initial configurations for diverse DDQCs, thereby opening possibilities for their discovery. Mathematically, a tiling is defined as a covering of a plane or space using one or more geometric shapes, called tiles, with no overlaps and no gaps. Therefore, different tiles and tiling rules (inflation rules) would result in different tilings. In what follows, we introduce the ST and QST tilings and construct a new DST tiling.

The ST tiling is a classical aperiodic tiling consisting of three types of triangles (T_s) and two types of squares (S_s), all with equal edge lengths. The inflation rule to construct ST tiling is discovered by Stampfli.[47] As shown in Figure 1a, the fundamental dodecagon (Figure 1a(I)) is transformed to the second-generation dodecagon (Figure 1a(III)) by following the inflation rules shown in Figure 1a(II). Here, the tiles obtained with different inflation rules are distinguished by different colors. The local third-generation pattern in Figure 1a(III) is obtained by inflating the T_1 and S_1 tiles twice. The corresponding edges of the three outlined S_1 are magnified by an inflation factor $\alpha = 2 + \sqrt{3}$ in each generation, where α is the platinum number, corresponding to the root of $f(x) = x^2 - 4x + 1$. Meanwhile, the substitution rule {AABA → A′, ABA → B′} is repeatedly applied to generate an aperiodic sequence. The "letters" A and B are two spacings between parallel lines passing through the vertices of the first-generation tiling, and A' and B' are the spacings between parallel lines passing through the vertices of the second-generation tiling. The length ratios between A' and A, and between B' and B are both α. The inflation matrix is given in the Supporting Information (SI), Section S1. The maximum eigenvalue of the inflation matrix is α^2.

The DST tiling, consisting of two kinds of T_s, two kinds of S_s, and one kind of diamond D, is a novel dodecagonal aperiodic tiling constructed in the current study. All of the prototiles have equal edge length, and their inflation rules are given in Figure 1b(II). The shape characteristic of diamond D is specified in Figure 1b(V). The fundamental dodecagon shown in Figure 1b(I) containing 6 T_1, 2 T_2, 2 D, 2 S_1, and 4 S_2 can inflate once to form a second-generation tiling; see Figure 1b(III). Meanwhile, the third-generation pattern is obtained by inflating the first-generation T_1, D, and S_2 twice. The first-, second-, and third-generation T_s are highlighted in black, arranged from bottom to top. Each generation can be magnified by a factor of α relative to the previous generation. Based on the inflation rule shown in Figure 1b(II), the number of these tiles in the $(n+1)$th generation, denoted by T_1^{n+1}, T_2^{n+1}, D^{n+1}, S_1^{n+1}, and S_2^{n+1}, are related to those in the nth generation by the inflation matrix M_{DST}

$$\begin{bmatrix} T_1^{n+1} \\ T_2^{n+1} \\ D^{n+1} \\ S_1^{n+1} \\ S_2^{n+1} \end{bmatrix} = \begin{bmatrix} 4 & 3 & 6 & 8 & 8 \\ 1 & 2 & 4 & 4 & 4 \\ 1 & 1 & 2 & 2 & 2 \\ 2 & 1 & 2 & 3 & 2 \\ 1 & 2 & 4 & 4 & 5 \end{bmatrix} \begin{bmatrix} T_1^{n} \\ T_2^{n} \\ D^{n} \\ S_1^{n} \\ S_2^{n} \end{bmatrix} := M_{DST} \begin{bmatrix} T_1^{n} \\ T_2^{n} \\ D^{n} \\ S_1^{n} \\ S_2^{n} \end{bmatrix} \quad (1)$$

Here, the inflation matrix M_{DST} keeps track of the number of various prototiles in a self-similar way, and its maximum eigenvalue is also α^2. If only the shape (T, D, and S) of the prototiles is distinguished, the inflation matrix can be simplified as

$$\begin{bmatrix} T^{n+1} \\ D^{n+1} \\ S^{n+1} \end{bmatrix} = \begin{bmatrix} 5 & 10 & 12 \\ 1 & 2 & 2 \\ 3 & 6 & 7 \end{bmatrix} \begin{bmatrix} T^{n} \\ D^{n} \\ S^{n} \end{bmatrix} \quad (2)$$

Furthermore, the vertices of the given generation tilings lying on the set of parallel lines can form two spacings ("letters") A and B, as shown in Figure 1b(III). These letters constitute an aperiodic sequence following the substitution rule {ABAA → A′, ABA → B′}, and the length ratios between A' and A, and between B' and B are both given by α. Note that the ST and DST tilings are incongruent tilings; the constituent tiles are not the same, and they are not related by plane rotations with no deformations. The tilings are certainly related, but the symmetry of the DST tiling is lower than that of the ST tiling. It is noted that the 12-fold "cogwheel" of the DST tiling in Figure 1b(I) has only two orthogonal mirror planes, along the vertical and horizontal directions, due to the two blue diamonds in the central hexagon. In contrast, the ST tiling consists of a central hexagon formed by six triangular tiles, which inherently results in six mirror planes.

The prototiles of either the ST or DST tilings are equilateral polygons. By introducing an incongruent quadrangle (Figure 1c(V)), we can construct the QST tiling, where the fundamental dodecagon is illustrated in Figure 1c(I). Figure 1c(II) displays nine prototiles and the corresponding inflation rules, containing four kinds of triangles T_1, T_2, T_3, and T_4, four kinds of quadrangles Q_1, Q_2, Q_3, and Q_4, and one kind of square S. A second-generation QST tiling with the third-generation of 1 Q_2, 1 Q_4, and 1 S is shown in Figure 1c(III). Three black-outlined Q_4 are self-similar, which are magnified by α from the bottom to top. The "letters" A and B form the same aperiodic sequence following the substitution rule {ABAA → A′, ABA → B′} as DST tiling. By tracking the changes in the number of T_1, T_2, T_3, T_4, S, Q_1, Q_2, Q_3, and Q_4 based on inflation rules, we can obtain the inflation matrix M_{QST}

https://doi.org/10.1021/acs.macromol.4c02380
Macromolecules 2025, 58, 5229−5239

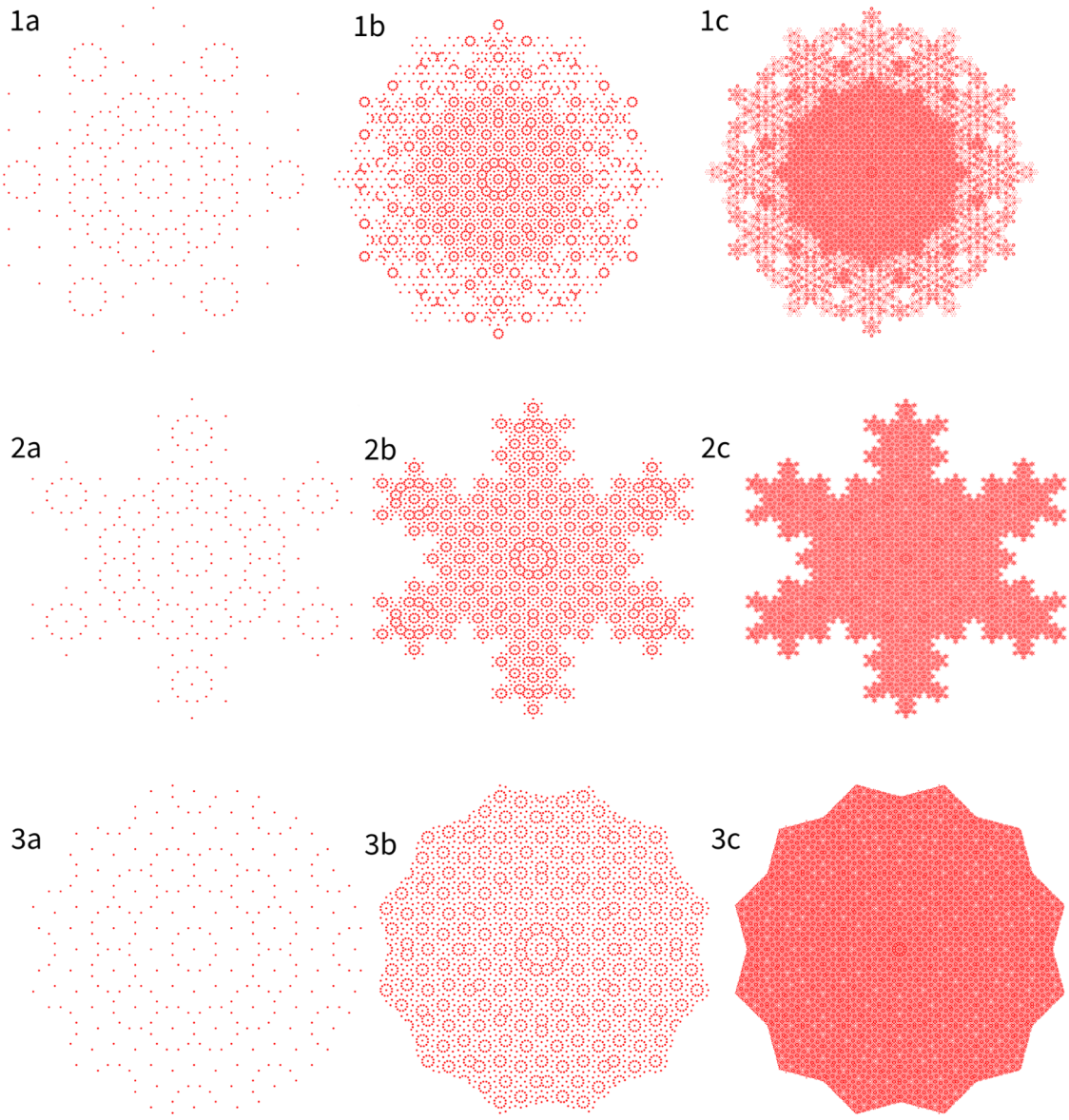

Figure 2. Higher-dimensional analysis of (1) ST tiling, (2) DST tiling, and (3) QST tiling. (a−c) Projection windows obtained by mapping second-to fourth-generation tilings to the perpendicular space.

$$M_{QST} = \begin{bmatrix} 1 & 1 & 2 & 3 & 1 & 0 & 0 & 1 & 1 \\ 2 & 2 & 5/2 & 3 & 2 & 2 & 1 & 5/2 & 3/2 \\ 0 & 0 & 0 & 0 & 2 & 0 & 1 & 0 & 1 \\ 1 & 1 & 1 & 1 & 1 & 1 & 1 & 1 & 1 \\ 3 & 3 & 3 & 3 & 5 & 7/2 & 7/2 & 7/2 & 7/2 \\ 2m & 2m & 0 & 0 & 4n & 2+2m & 2m & 1+m & m \\ 0 & 0 & m & 0 & 4 & 0 & 1 & 1 & 1 \\ m & m & 0 & 0 & 2m+4n & 1+m & 1+m & 1+m/2 & m/2 \\ 0 & 0 & m/2 & 0 & 4 & 0 & 1 & 0 & 2 \end{bmatrix}$$

During the inflation process, the contribution of Q in all prototiles manifests not only as a whole but also in the form of divided equilateral triangle and right triangle, as indicated by the dashed lines in Figure 1c(V). Thus, the area ratios $m = 2\sqrt{3}/(1 + 2\sqrt{3})$ and $n = 1/(1 + 2\sqrt{3})$ of the two parts relative to Q are used to describe the contribution of Q, respectively. The maximum eigenvalue of M_{QST} is also α^2.

https://doi.org/10.1021/acs.macromol.4c02380
Macromolecules 2025, 58, 5229−5239

To better understand these dodecagonal tilings, a high-dimensional analysis is carried out by using the classical cut-and-project method.[48] This involves representing a low-dimensional QC as a projection of a high-dimensional crystal onto a two-dimensional physical space. The high-dimensional space is divided into parallel and perpendicular spaces. By mapping the vertices of the second-, third-, and fourth-generation tilings to the perpendicular space, we construct their projection windows shown in Figure 2. The windows of the ST and DST tilings exhibit fractal characteristics. The DST tiling window resembles a Koch snowflake, and the QST tiling window resembles the shape of two overlapping hexagons. The Hausdorff dimension of the projection window for DST tiling is $\log 6/\log(2 + \sqrt{3}) \approx 1.3605$, while the Hausdorff dimensions of the projection windows for the ST and QST tilings are still unknown. It is noted that the different windows for the ST and DST tiling in Figure 2 also highlight the differences between the DST and ST tilings.

SCFT OF T-SHAPED LIQUID CRYSTALLINE MOLECULES

For a given molecular system, we solve the SCFT equations using various initial configurations, including the dodecagonal tilings, to obtain solutions corresponding to the different ordered phases. The free energies of these phases are then used to analyze their relative stability. The first step of the SCFT procedure is to develop an SCFT framework for the given molecular systems.

In this study, we consider an incompressible melt of n T-shaped pentablock terpolymers (Figure 3) with an overall

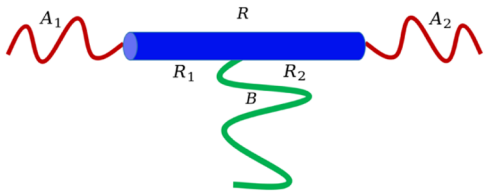

Figure 3. T-shaped liquid crystalline molecule consisting of a rigid rod R (blue) with two flexible blocks, A_1 and A_2 (red), tethered at its ends and a flexible side block B (green).

degree of polymerization or number of segments N in a volume of V. Each TLCM consists of a liquid crystalline (rigid rod) middle block R (blue) with two flexible end blocks, A_1 and A_2 (red), tethered at the ends of the rod and one flexible side block B (green) grafted at the middle of the rod. The grafting point of the B block divides the rod R block into two, R_1 and R_2, subblocks. Effectively, the TLCM is a pentablock copolymer with five blocks, $\alpha = \{A_1, A_2, B, R_1, \text{and } R_2\}$. The volume fraction of the α-block is denoted by f_α with $\alpha = \{A_1, A_2, B, R_1, \text{and } R_2\}$. For the TLCM specified in Figure 3, the volume fractions are given by, $f_{A_2} = \epsilon_A f_{A_1}, f_{R_2} = \epsilon_R f_{R_1}$, with $\sum_\alpha f_\alpha = 1$.

We model the flexible blocks as Gaussian chains and the rigid blocks as wormlike chains. Within the SCFT framework, the free energy per TLCM in units of thermal energy k_BT, where T is the temperature and k_B is the Boltzmann constant, can be expressed as[38]

$$
\begin{aligned}
f &= \frac{F}{nk_BT} \\
&= \frac{1}{V}\int_V \left[\frac{1}{4N\zeta_1}\mu_1^2(\boldsymbol{r}) + \frac{1}{4N\zeta_2}\mu_2^2(\boldsymbol{r}) - \mu_+(\boldsymbol{r})\right] d\boldsymbol{r} \\
&\quad + \frac{1}{2\eta NV}\int_V \mathcal{M}(\boldsymbol{r}) : \mathcal{M}(\boldsymbol{r}) d\boldsymbol{r} - \log Q,
\end{aligned} \tag{3}
$$

where the Maier−Saupe interaction parameter η quantifies the strength of the orientational interaction favoring the alignment of the rod blocks, Q is the single-chain partition function. The symbol $A : B$ denotes the double dot product, defined as $A : B = \sum_{ij} A_{ij}B_{ij}$. μ_1 and μ_2 are the general "exchange chemical potential" of the system. μ_+ is the pressure potential to ensure local incompressibility. $\mathcal{M}$ is the orientational field of the semiflexible chain. The parameters ζ_1 and ζ_2 are related to the interactions between different blocks

$$
\zeta_1 = \frac{2\chi_{AB}\chi_{AR} + 2\chi_{AB}\chi_{BR} + 2\chi_{AR}\chi_{BR} - \chi_{AB}^2 - \chi_{AR}^2 - \chi_{BR}^2}{4\chi_{AB}}, \quad \zeta_2 = \chi_{AB}
$$

where $\chi_{\alpha\beta}$ is the Flory−Huggins interaction parameter between the α and β blocks. The mean fields for the different blocks, $w_\alpha(\boldsymbol{r})$, $\alpha \in \{A, B, \text{and } R\}$, are linear combinations of the μ-fields, $w_\alpha = \mu_+ - \sigma_{1\alpha}\mu_1 - \sigma_{2\alpha}\mu_2$, where the σ-coefficients are given by

$$
\begin{aligned}
&\sigma_{1A} = \frac{1}{3}, \sigma_{1R} = -\frac{2}{3}, \sigma_{1B} = \frac{1}{3}, \\
&\sigma_{2A} = \frac{1+\alpha}{3}, \sigma_{2R} = \frac{1-2\alpha}{3}, \sigma_{2B} = \frac{\alpha-2}{3}, \\
&\alpha = \frac{\chi_{AB} + \chi_{AR} - \chi_{BR}}{2\chi_{AB}}
\end{aligned}
$$

The single-chain partition function Q, the density distribution of different blocks, ϕ_α ($\alpha = \{A, B, R\}$), and the orientation order parameter $\mathcal{S}$ are computed from the chain propagators, $q_\alpha(\boldsymbol{r}, s)$ and $q_\alpha^\dagger(\boldsymbol{r}, s)$, $\alpha = \{A_1, A_2, B\}$, $q_\beta(\boldsymbol{r}, \boldsymbol{u}, s)$ and $q_\beta^\dagger(\boldsymbol{r}, \boldsymbol{u}, s)$, $\beta = \{R_1, R_2\}$, which in turn are obtained by solving a set of modified diffusion equations (MDEs). Here, $\boldsymbol{u}$ is a vector defined on the unit sphere $\mathcal{S}$, which represents the local orientation of the semiflexible molecule. Specifically, we have

https://doi.org/10.1021/acs.macromol.4c02380
Macromolecules 2025, 58, 5229−5239

$$Q = \frac{1}{V}\int_V q_B(\boldsymbol{r}, s)q_B^{\dagger}(\boldsymbol{r}, s)d\boldsymbol{r},\ \forall\ s \in [0, f_B].$$

$$\phi_A(\boldsymbol{r}) = \frac{1}{Q}\left(\int_0^{f_{A_1}} q_{A_1}(\boldsymbol{r}, s)q_{A_1}^{\dagger}(\boldsymbol{r}, s)\mathrm{d}s + \int_0^{f_{A_2}} q_{A_2}(\boldsymbol{r}, s)q_{A_2}^{\dagger}(\boldsymbol{r}, s)\mathrm{d}s\right),$$

$$\phi_B(\boldsymbol{r}) = \frac{1}{Q}\int_0^{f_B} q_B(\boldsymbol{r}, s)q_B^{\dagger}(\boldsymbol{r}, s)\mathrm{d}s,$$

$$\phi_R(\boldsymbol{r}) = \frac{2\pi}{Q}\left(\int_0^{f_{R_1}}\int_S q_{R_1}(\boldsymbol{r}, \boldsymbol{u}, s)q_{R_1}^{\dagger}(\boldsymbol{r}, \boldsymbol{u}, s)d\boldsymbol{u}\mathrm{d}s + \int_0^{f_{R_2}}\int_S q_{R_2}(\boldsymbol{r}, \boldsymbol{u}, s)q_{R_2}^{\dagger}(\boldsymbol{r}, \boldsymbol{u}, s)d\boldsymbol{u}\mathrm{d}s\right),$$

$$\mathcal{S}(\boldsymbol{r}) = \frac{2\pi}{Q}\left(\int_0^{f_{R_1}}\int_S q_{R_1}(\boldsymbol{r}, \boldsymbol{u}, s)\left(\boldsymbol{uu} - \frac{1}{2}\boldsymbol{I}\right)q_{R_1}^{\dagger}(\boldsymbol{r}, \boldsymbol{u}, s)d\boldsymbol{u}\mathrm{d}s + \int_0^{f_{R_2}}\int_S q_{R_2}(\boldsymbol{r}, \boldsymbol{u}, s)\left(\boldsymbol{uu} - \frac{1}{2}\boldsymbol{I}\right)q_{R_2}^{\dagger}(\boldsymbol{r}, \boldsymbol{u}, s)d\boldsymbol{u}\mathrm{d}s\right) \tag{4}$$

Here, $q_\alpha(\boldsymbol{r}, s)$, $\alpha \in \{A_1, A_2, B\}$ is the forward propagator, representing the probability of finding the sth α segment at a spatial position $\boldsymbol{r}$ from $s = 0$ to $s = f_\alpha$ under mean field w_α. The backward propagator $q_\alpha^{\dagger}(\boldsymbol{r}, s)$ represents the probability weight from $s = f_\alpha$ to $s = 0$. For the Gaussian chains, the propagators satisfy the modified diffusion equations (MDEs)[39]

$$\frac{\partial}{\partial s}q_\alpha(\boldsymbol{r}, s) = \nabla_{\boldsymbol{r}}^2 q_\alpha(\boldsymbol{r}, s) - w_\alpha(\boldsymbol{r})q_\alpha(\boldsymbol{r}, s),\ 0 \le s \le f_\alpha,$$

$$q_\alpha(\boldsymbol{r}, 0) = 1.$$

$$\frac{\partial}{\partial s}q_\alpha^{\dagger}(\boldsymbol{r}, s) = \nabla_{\boldsymbol{r}}^2 q_\alpha^{\dagger}(\boldsymbol{r}, s) - w_\alpha(\boldsymbol{r})q_\alpha^{\dagger}(\boldsymbol{r}, s),\ 0 \le s \le f_\alpha,$$

$$q_B^{\dagger}(\boldsymbol{r}, 0) = \int_S q_{R_1}(\boldsymbol{r}, \boldsymbol{u}, f_{R_1})q_{R_2}(\boldsymbol{r}, \boldsymbol{u}, f_{R_2})d\boldsymbol{u}.$$

$$q_{A_1}^{\dagger}(\boldsymbol{r}, 0) = \int_S q_{R_1}^{\dagger}(\boldsymbol{r}, \boldsymbol{u}, f_{R_1})d\boldsymbol{u},$$

$$q_{A_2}^{\dagger}(\boldsymbol{r}, 0) = \int_S q_{R_2}^{\dagger}(\boldsymbol{r}, \boldsymbol{u}, f_{R_2})d\boldsymbol{u} \tag{5}$$

For semiflexible chains, the forward propagators $q_\beta(\boldsymbol{r}, \boldsymbol{u}, s)$ and $\beta \in \{R_1, R_2\}$ represent the probability of the end point of the s segment at spatial position $\boldsymbol{r}$ and orientational position $\boldsymbol{u}$. They satisfy the "convective diffusion" equations[39]

$$\frac{\partial}{\partial s}q_\beta(\boldsymbol{r}, \boldsymbol{u}, s) = -\nu\boldsymbol{u}\cdot\nabla_{\boldsymbol{r}}q_\beta(\boldsymbol{r}, \boldsymbol{u}, s) - \Gamma(\boldsymbol{r}, \boldsymbol{u})q_\beta(\boldsymbol{r}, \boldsymbol{u}, s) + \frac{1}{2\lambda}\nabla_{\boldsymbol{u}}^2 q_\beta(\boldsymbol{r}, \boldsymbol{u}, s),$$

$$q_{R_1}(\boldsymbol{r}, \boldsymbol{u}, 0) = \frac{q_{A_1}(\boldsymbol{r}, f_{A_1})}{2\pi},\ 0 \le s \le f_{R_1},$$

$$q_{R_2}(\boldsymbol{r}, \boldsymbol{u}, 0) = \frac{q_{A_2}(\boldsymbol{r}, f_{A_2})}{2\pi},\ 0 \le s \le f_{R_2}, \tag{6}$$

where $\Gamma(\boldsymbol{r}, \boldsymbol{u}) = w_R(\boldsymbol{r}) - \mathcal{M}(\boldsymbol{r})$: $\left(\boldsymbol{uu} - \frac{1}{2}\boldsymbol{I}\right)$. The parameter $\nu = (b_R/b_B)(6N)^{1/2}$ measures the size asymmetry of monomers R and B, b_A and b_B represent the statistical segment lengths of monomers A and B, respectively. λ is the hardness of the semiflexible chain. The backward propagators of the semiflexible block satisfy

$$\frac{\partial}{\partial s}q_\beta^{\dagger}(\boldsymbol{r}, \boldsymbol{u}, s) = \nu\boldsymbol{u}\cdot\nabla_{\boldsymbol{r}}q_\beta^{\dagger}(\boldsymbol{r}, \boldsymbol{u}, s) - \Gamma(\boldsymbol{r}, \boldsymbol{u})q_\beta^{\dagger}(\boldsymbol{r}, \boldsymbol{u}, s) + \frac{1}{2\lambda}\nabla_{\boldsymbol{u}}^2 q_\beta^{\dagger}(\boldsymbol{r}, \boldsymbol{u}, s),$$

$$q_{R_1}^{\dagger}(\boldsymbol{r}, \boldsymbol{u}, 0) = \frac{1}{2\pi}q_B(\boldsymbol{r}, f_B)q_{R_2}(\boldsymbol{r}, \boldsymbol{u}, f_{R_2}),\ 0 \le s \le f_{R_1},$$

$$q_{R_2}^{\dagger}(\boldsymbol{r}, \boldsymbol{u}, 0) = \frac{1}{2\pi}q_B(\boldsymbol{r}, f_B)q_{R_1}(\boldsymbol{r}, \boldsymbol{u}, f_{R_1}),\ 0 \le s \le f_{R_2} \tag{7}$$

Finally, the various fields and densities are related by the self-consistent equations that are obtained by the minimization conditions

$$\frac{\delta f}{\delta \mu_+} = \phi_A + \phi_B + \phi_R - 1 = 0,$$

$$\frac{\delta f}{\delta \mu_1} = \frac{1}{2N\zeta_1}\mu_1 - \sigma_{1A}\phi_A - \sigma_{1R}\phi_R - \sigma_{1B}\phi_B = 0,$$

$$\frac{\delta f}{\delta \mu_2} = \frac{1}{2N\zeta_2}\mu_2 - \sigma_{2A}\phi_A - \sigma_{2R}\phi_R - \sigma_{2B}\phi_B = 0,$$

$$\frac{\delta f}{\delta M} = \frac{1}{\eta N}\mathcal{M} - \mathcal{S} = 0 \tag{8}$$

Mathematically, the SCFT of LCMs is a nonlocal, multisolution, multiparameter, high-dimensional, and nonlinear variational problem. The solutions of SCFT are saddle points of the free energy landscape corresponding to different ordered structures. Obtaining these solutions numerically requires a diverse set of initial configurations and accurate algorithms. In order to study the relative stability of QCs, it is essential to construct initial configurations corresponding to various DDQCs as well as periodic structures. The initial configurations for DDQCs can be obtained by constructing dodecagonal aperiodic tilings. There exists a gap between these aperiodic tilings, which is a geometric construction, and the density profiles of candidate phases for SCF calculations. To bridge this gap, we employ a method to decorate tilings with smooth functions like Gaussian or tanh function (eq S3). Specifically, the density functions ϕ_A and ϕ_B are obtained by decorating the dodecagonal tilings and their dual tilings (red and green vertices in Figure 1(IV)), respectively, while ϕ_R is obtained by using the incompressibility condition. Using this approach, the initial configurations of three DDQCs, namely, the square−triangle DDQC (STQC), diamond−square−triangle DDQC (DSTQC), and quadrangle−square−triangle DDQC (QSTQC) can be obtained. Their corresponding converged states are illustrated in Figure 5, and the white lines are a rough guide for the tiling pattern of the converged structure. Since the initial configuration might change during SCFT iteration, the converged configuration does not always perfectly match the initial tiling pattern.

Accurate and efficient algorithms are required to solve the SCFT equations. In this work, we consider two-dimensional

https://doi.org/10.1021/acs.macromol.4c02380
Macromolecules 2025, 58, 5229−5239

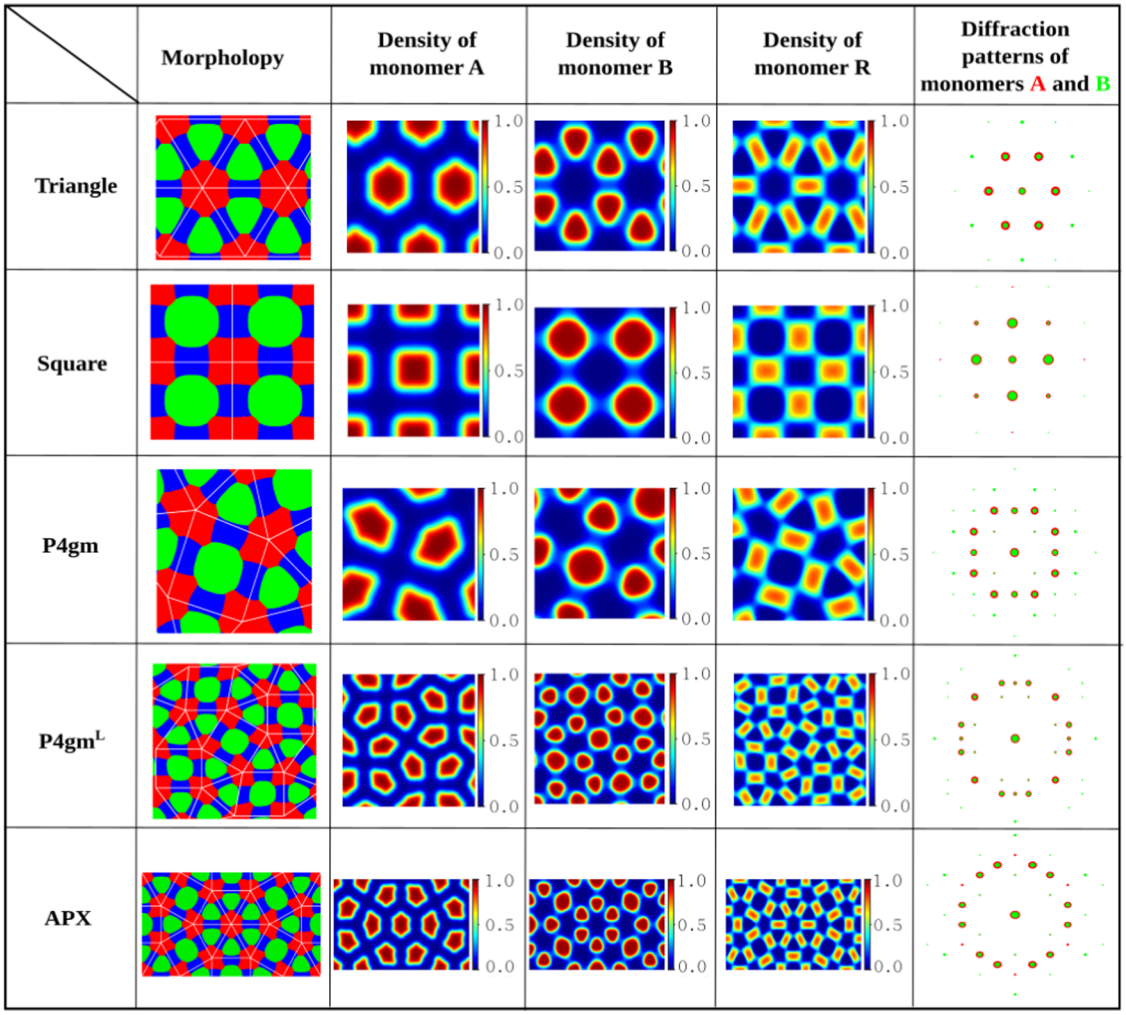

Figure 4. Periodic phases self-assembled from TLCMs. The second column presents the morphologies in which A-, B-, and R-rich domains are plotted in red, green, and blue colors, respectively. The white lines are a rough guide for the tiling pattern of the converged structure. The third, fourth, and fifth columns show the density distributions of components A, B, and R, respectively. The last column shows the main diffraction peaks of components A (red) and B (green).

ordered structures and restrict the orientation of the rigid block on a unit circle; i.e., the orientation of the rigid rods is represented by the polar angle $\theta \in [0, 2\pi]$. After comparing the accuracy and efficiency of various numerical algorithms, we use the Fourier pseudospectral method to discrete spatial and orientational variables, the fourth-order backward difference formula and the fourth-order Runge−Kutta method to discrete the contour variable of Gaussian and Wormlike chain propagators, respectively. And the hybrid nonlinear iteration scheme is used to find the saddle points of the SCFT.[49] During the self-consistent iteration, we utilize optimization algorithms to relax the calculation domain to allow the structures to reach their optimal energy states. For more algorithmic details and procedures, please refer to the SI, Section S3. Meanwhile, a parallel technique is developed using FFTW-MPI package in C ++ language[50] to accelerate the calculations.

SCFT SOLUTIONS OF DDQCS

Using aperiodic tilings as initial configurations allowed us to obtain SCFT solutions of three DDQCs shown in Figure 4. The self-consistency of all of the SCFT solutions is determined by demanding that the free energy difference between consecutive iteration steps is less than the iteration tolerance of tol = 1.0×10^{-8}. The relative stability of all candidate phases is examined by using their free energies. Phase diagram of the system is constructed by a comparison of the free energies of the candidate phases. The library of candidate phases used in the current study includes the three DDQCs and their crystal approximants, such as P4gm, APX,[4] P4gm^L,[8] as well as polygonal structures including the triangle and square. The corresponding diffraction patterns of each phase are displayed in Figures 4 and 5. Specifically, STQC exhibits more prominent diffraction peaks compared with DSTQC, as it maintains a higher rotational symmetry and greater self-similarity.

Previous experiments and simulations have revealed that the DDQCs could form between the stable regions of the triangular and quadrangular phases.[23−25,28−30] For the case of TLCMs, our previous SCFT calculations[51] have provided a suitable parametric range for the search of stable DDQCs, *i.e.*, $\epsilon_A = 0.4$, $f_{R_1} = 0.14$, $\epsilon_R = 1.1$, $\eta = 0.3$, $b_A = b_B = 1.0$, and $\lambda = 300$. Due to the significant impact of Flory−Huggins parameters χ_{AR}, χ_{BR}, χ_{AB}, and the side chain length f_B on phase stability, we employ $\chi = \chi_{AR}$ ($\chi_{BR} = \chi - 0.02$, $\chi_{AB} = \chi - 0.04$) to analyze the stability of three DDQCs. Comparing the SCFT free energies of all ordered phases with fixed parameters,

https://doi.org/10.1021/acs.macromol.4c02380
Macromolecules 2025, 58, 5229−5239

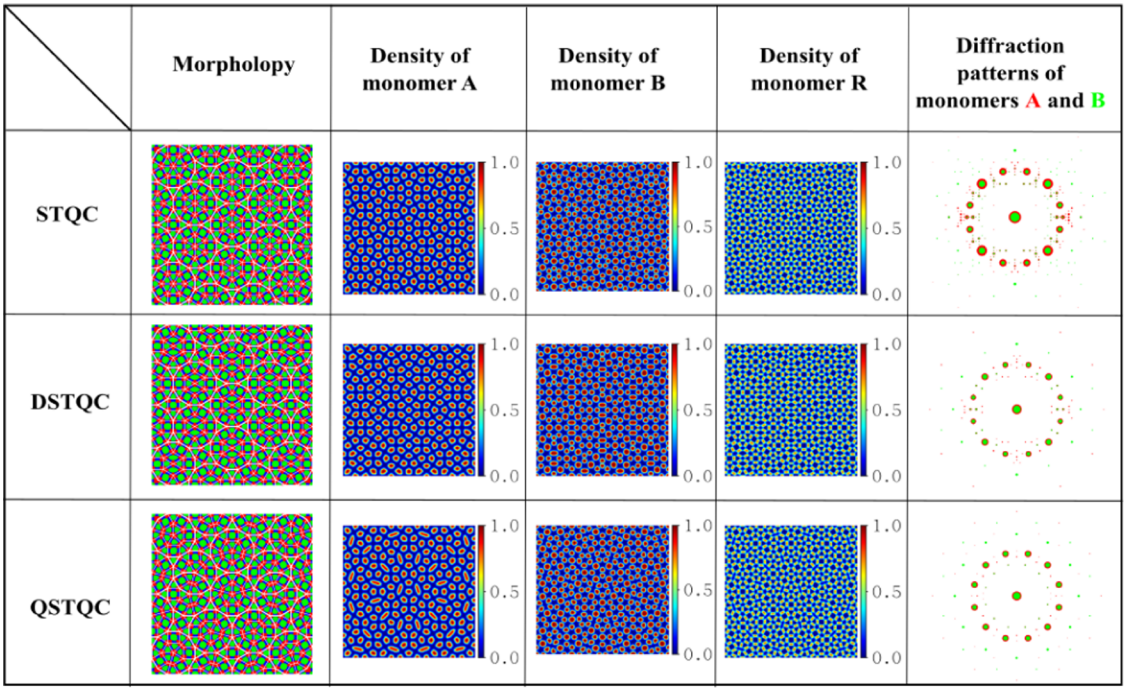

Figure 5. DDQCs self-assembled from TLCMs. The second column presents the morphologies in which A-, B-, and R-rich domains are plotted in red, green, and blue colors, respectively. The white lines are a rough guide for the tiling pattern of the converged structure. The third, fourth, and fifth columns show the density distributions of components A, B, and R, respectively. The last column shows the main diffraction peaks of components A (red) and B (green).

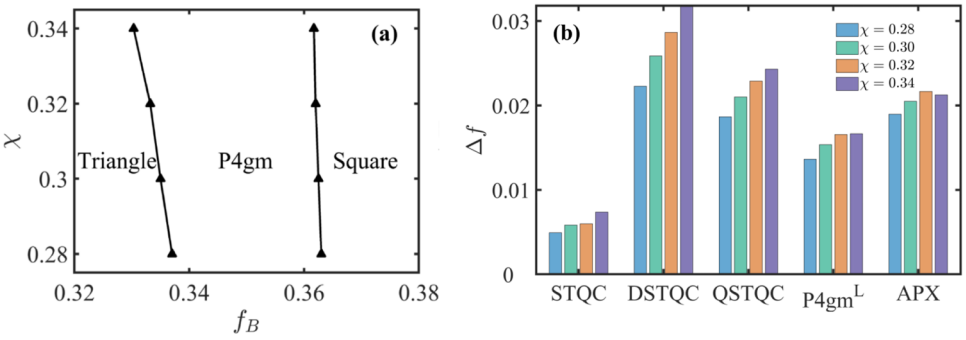

Figure 6. (a) Phase diagram in the $\chi - f_B$ plane. Symbols indicate the transition points determined by SCFT; while solid lines are a guide for the eyes. (b) Free energy differences $\Delta f = f - f_{\mathrm{P4gm}}$ at $[\chi - f_B] = [0.28 - 0.351]$, $[0.30 - 0.350]$, $[0.32 - 0.348]$, and $[0.34 - 0.347]$. Here, the parameters are $\epsilon_A = 0.4$, $f_{R_1} = 0.14$, $\epsilon_R = 1.1$, $\eta = 0.3$, and $\lambda = 300$.

the one with the lowest free energy is taken as the stable structure at that point. The resulting phase diagram in the χ-f_B plane is presented in Figure 6a. This phase diagram shows that in the range of $\chi \in [0.28, 0.34]$, the DDQCs are metastable phases that do not appear in the phase diagram. A phase transition sequence from triangle, to P4gm, and then to square is observed when f_B is increased. These stable phases are either congruent triangle/square tilings or their combination (P4gm). The three QCs, STQC, DSTQC, and QSTQC, are all solutions of the SCFT equations but they are metastable states within the parameter range. It is worth noticing that the free energy differences per chain between the DDQCs and their crystalline approximants (P4gm, P4gm^{L}) are quite small, at the 10^{-2} level, as shown in Figure 6b.

In order to understand the influence of different factors on the relative stability of the ordered phases, we divide the free energy per chain into three parts: interaction energy (f_I), orientation interaction energy (f_M), and entropic contribution (f_E)

$$f = \underbrace{\frac{1}{V}\int_V \left(\frac{1}{4N\zeta_1}\mu_1^2 + \frac{1}{4N\zeta_2}\mu_2^2 - \mu_+\right)\boldsymbol{dr}}_{f_I} + \underbrace{\frac{1}{2\eta NV}\int_V \mathcal{M}(\boldsymbol{r}):\mathcal{M}(\boldsymbol{r})\boldsymbol{dr}}_{f_M} - \underbrace{\log Q}_{f_E} \tag{9}$$

An example of these free energy components with $\chi = 0.30$ and $\eta = 0.35$ is shown in Figure 7. The numerical results from SCFT calculations indicate that the DDQCs have lower f_I and f_M values compared to those of the stable P4gm. However, the relatively larger contribution of f_E prevents the DDQCs become stable phases, despite the advantage brought by the f_I and f_M. Thus, the entropic contribution f_E dominates the

https://doi.org/10.1021/acs.macromol.4c02380
Macromolecules 2025, 58, 5229−5239

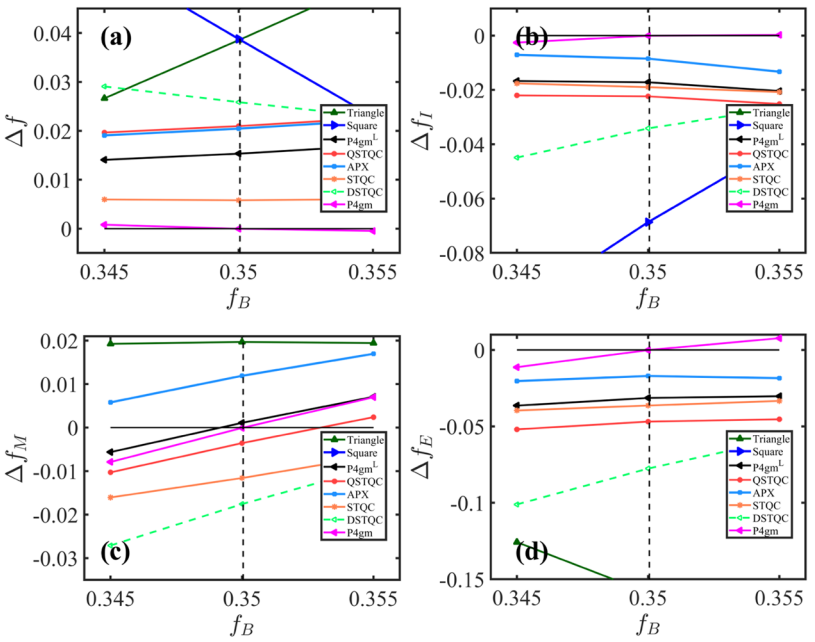

Figure 7. (a–d) Free energy difference per chain $\Delta f = f - f_{P4gm}$ among all phases with $\chi = \chi_{AR} = 0.30$, where f_{P4gm} is the free energy per chain of P4gm on the boundary of triangle and square indicated by dashed lines. (b–d) Three parts energy differences correspond to panel (a).

stability of DDQCs. Similarly, the DDQCs are metastable phases for the Maier–Saupe parameter in the range of $\eta \in [0.3, 0.36]$. The corresponding phase diagram and free energy components (in the SI, Section S4) confirm the dominant role of f_E in stabilizing the different phases.

One interesting question is whether the introduction of randomness to the DDQCs can alter the entropic contribution to the free energy f_E, thus enhancing their stability. There are two ways to introduce randomness to construct random tilings for the DDQC morphologies. The first one is the zipper update move approach,[52] which can disrupt the self-similarity through the phase flipping mechanism. The imperfect aperiodic tilings obtained by this method are almost degenerate compared with the DDQCs, as indicated by the observation that their free energies are nearly equal.[53] This method has already been applied in the construction of random STQC in the SCFT calculations of ABCB tetrablock copolymers, resulting in metastable structures with free energy variation per chain only at the 10^{-3} level.[4] The conclusion from these studies is that the zipper update method could not increase f_E sufficiently to stabilize the DDQCs. The second one is randomly rotating the fundamental dodecagon in DDQCs such that they still guarantee dodecagonal symmetry, as shown in Figure S2. This method could either increase or decrease the energy f_E. For instance, in the STQC-R1 tiling, rotation increases f_E, while in the QSTQC-R1 tiling, it decreases f_E. However, the free energy variations per chain resulting from rotation are also only very small at the 10^{-3} level, as shown in Figure S3. Therefore, the randomness through rotation still does not increase f_E enough to stabilize the DDQCs in the TLCMs. Discrepancies between theoretical and experimental results may arise from the challenges in accurately simulating experimental systems, such as polymer systems with ions, which are difficult to model with SCFT.[8]

Based on these SCFT studies, it can be concluded that the stability of the DDQCs obtained via the inflation rules and their randomized variations are insensitive to the parameters χ, η, and f_B of the TLCMs. Therefore, in the future, we should attempt to introduce more blocks or blends into the system to modulate the energy and achieve stable DDQCs.

DISTINGUISHING DIVERSE DDQCS AND THEIR APPROXIMANTS

The three DDQCs and their approximants exhibit similar symmetries, as shown in Figure 8. The common method of

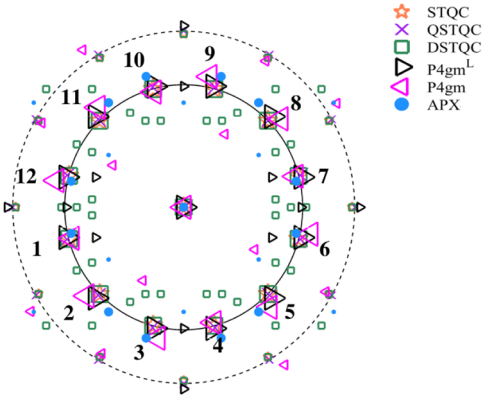

Figure 8. Diffraction peaks of monomer A for DDQCs and their approximants when $\chi = 0.30$ and $f_B = 0.35$. The solid circle represents the location of first-order diffraction peaks, and the dashed circle shows the location of some second-order diffraction peaks.

identifying ordered structures through different symmetries of diffraction peaks[1,6] requires further developing. We can arrange the diffraction peaks in the descending order based on their symmetry and the magnitude of their Fourier coefficients. The Fourier coefficients are calculated by the standard expression.[39] We designate the top 12 peaks as the first-order peaks, while the subsequent peaks, ranked from 13 to 24, as the second-order peaks. Based on this, we combine the positions of the first-order with the second-order peaks to achieve this task. Focusing on the positions of the A diffraction peaks when $\chi =$

https://doi.org/10.1021/acs.macromol.4c02380
Macromolecules 2025, 58, 5229–5239

0.30, f_B = 0.35, as shown in Figure 8, it is evident that the overlapping first-order peaks (lie on solid circle) are difficult to distinguish between DDQCs and their approximants, except for APX. However, when combined with nonoverlapping second-order peaks position (lie on dashed circle), it is sufficient to distinguish all structures. More detailed position comparisons are shown in Table S2. The criterion is presented for the parameter χ = 0.30, f_B = 0.35 as an example, and it is applicable to other parameters.

CONCLUSIONS

In summary, we constructed three dodecagonal aperiodic tilings, including a novel DST tiling, and used them to construct initial density profiles for the SCFT. By applying the cut-and-project method, we showed that the aperiodic tilings could be obtained from the projection of higher-dimensional periodic lattice points to the lattice points of parallel space within a projection window. The availability of the initial configurations allowed us to obtain accurate solutions of the SCFT equations corresponding to metastable DDQCs. A free energy analysis underscored the dominant role of the entropic contribution to the free energy in determining the stability of the DDQCs. We also showed that the introduction of random-tiling DDQCs is insufficient to stabilize the DDQCs. These insights highlight the need to explore additional mechanisms that can stabilize the DDQCs, such as adjusting the molecular topology and introducing extra species via blending. For three DDQCs and their approximants, we provided a criterion to distinguish them based on diffraction peaks. This work represents an effort to investigate DDQCs within the SCFT framework of TLCMs. The methodology and results from the current study not only open new possibilities for research on soft QCs but also provide guidance for experimental investigations aimed at discovering novel DDQCs.

ASSOCIATED CONTENT

Supporting Information

The Supporting Information is available free of charge at https://pubs.acs.org/doi/10.1021/acs.macromol.4c02380.

Aperiodic tilings, random DDQCs, numerical methods, effects of χ and η on the thermodynamic stability, and diffraction peaks (PDF)

AUTHOR INFORMATION

Corresponding Authors

An-Chang Shi − *Department of Physics and Astronomy, McMaster University, Hamilton, Ontario L8S4M1, Canada;* orcid.org/0000-0003-1379-7162; Email: shi@mcmaster.ca

Pingwen Zhang − *School of Mathematics and Statistics, Wuhan University, Wuhan 430072, China; School of Mathematical Sciences, Peking University, Beijing 100871, China*; Email: pzhang@pku.edu.cn

Kai Jiang − *Hunan Key Laboratory for Computation and Simulation in Science and Engineering, Key Laboratory of Intelligent Computing and Information Processing of Ministry of Education, School of Mathematics and Computational Science, Xiangtan University, Xiangtan, Hunan 411105, China;* orcid.org/0000-0002-8035-3775; Email: kaijiang@xtu.edu.cn

Author

Xin Wang − *Hunan Key Laboratory for Computation and Simulation in Science and Engineering, Key Laboratory of Intelligent Computing and Information Processing of Ministry of Education, School of Mathematics and Computational Science, Xiangtan University, Xiangtan, Hunan 411105, China*

Complete contact information is available at: https://pubs.acs.org/10.1021/acs.macromol.4c02380

Notes

The authors declare no competing financial interest.

ACKNOWLEDGMENTS

This work is partially supported by the National Key R&D Program of China (2023YFA1008802), the National Natural Science Foundation of China (12171412 and 12288101), the Science and Technology Innovation Program of Hunan Province (2024RC1052), the Innovative Research Group Project of Natural Science Foundation of Hunan Province of China (2024JJ1008), the Natural Sciences and Engineering Research Council of Canada, and the High Performance Computing Platform of Xiangtan University.

REFERENCES

(1) Shechtman, D.; Blech, I.; Gratias, D.; Cahn, J. W. Metallic phase with long-range orientational order and no translational symmetry. *Phys. Rev. Lett.* **1984**, *53*, 1951.

(2) Steurer, W. Twenty years of structure research on quasicrystals. Part I. Pentagonal, octagonal, decagonal and dodecagonal quasicrystals. *Z. Kristallogr. - Cryst. Mater.* **2004**, *219*, 391−446.

(3) Gillard, T. M.; Lee, S.; Bates, F. S. Dodecagonal quasicrystalline order in a diblock copolymer melt. *Proc. Natl. Acad. Sci. U.S.A.* **2016**, *113*, 5167−5172.

(4) Duan, C.; Zhao, M.; Qiang, Y.; Chen, L.; Li, W.; Qiu, F.; Shi, A.-C. Stability of two-dimensional dodecagonal quasicrystalline phase of block copolymers. *Macromolecules* **2018**, *51*, 7713−7721.

(5) Suzuki, M.; Orido, T.; Takano, A.; Matsushita, Y. The largest quasicrystalline tiling with dodecagonal symmetry from a single pentablock quarterpolymer of the AB_1CB_2D type. *ACS Nano* **2022**, *16*, 6111−6117.

(6) Zeng, X.; Ungar, G.; Liu, Y.; Percec, V.; Dulcey, A. E.; Hobbs, J. K. Supramolecular dendritic liquid quasicrystals. *Nature* **2004**, *428*, 157−160.

(7) Zhang, R.; Zeng, X.; Ungar, G. Direct AFM observation of individual micelles, tile decorations and tiling rules of a dodecagonal liquid quasicrystal. *J. Phys.:Condens. Matter* **2017**, *29*, No. 414001.

(8) Zeng, X.; Glettner, B.; Baumeister, U.; Chen, B.; Ungar, G.; Liu, F.; Tschierske, C. A columnar liquid quasicrystal with a honeycomb structure that consists of triangular, square and trapezoidal cells. *Nat. Chem.* **2023**, *15*, 625−632.

(9) Talapin, D. V.; Shevchenko, E. V.; Bodnarchuk, M. I.; Ye, X.; Chen, J.; Murray, C. B. Quasicrystalline order in self-assembled binary nanoparticle superlattices. *Nature* **2009**, *461*, 964−967.

(10) Fischer, S.; Exner, A.; Zielske, K.; Perlich, J.; Deloudi, S.; Steurer, W.; Lindner, P.; Förster, S. Colloidal quasicrystals with 12-fold and 18-fold diffraction symmetry. *Proc. Natl. Acad. Sci. U.S.A.* **2011**, *108*, 1810−1814.

(11) Terasaki, O. *Mesoporous Crystals and Related Nano-structured Materials: Proceedings of the Meeting on Mesoporous Crystals and Related Nano-Structured Materials*; Elsevier, 2004; Vol. *148*.

(12) Johnston, J. C.; Phippen, S.; Molinero, V. A single-component silicon quasicrystal. *J. Phys. Chem. Lett.* **2011**, *2*, 384−388.

(13) Reinhardt, A.; Schreck, J. S.; Romano, F.; Doye, J. P. Self-assembly of two-dimensional binary quasicrystals: A possible route to a DNA quasicrystal. *J. Phys.:Condens. Matter* **2017**, *29*, No. 014006.

(14) Noya, E. G.; Wong, C. K.; Llombart, P.; Doye, J. P. How to design an icosahedral quasicrystal through directional bonding. *Nature* **2021**, *596*, 367−371.
(15) Nagaoka, Y.; Zhu, H.; Eggert, D.; Chen, O. Single-component quasicrystalline nanocrystal superlattices through flexible polygon tiling rule. *Science* **2018**, *362*, 1396−1400.
(16) Liu, Y.; Liu, T.; Yan, X.-Y.; Guo, Q.-Y.; Lei, H.; Huang, Z.; Zhang, R.; Wang, Y.; Wang, J.; Liu, F.; Bian, F.-G.; Meijer, E.; Aida, T.; Huang, M.; Cheng, S. Z. Expanding quasiperiodicity in soft matter: Supramolecular decagonal quasicrystals by binary giant molecule blends. *Proc. Natl. Acad. Sci. U.S.A.* **2022**, *119*, No. e2115304119.
(17) Iacovella, C. R.; Keys, A. S.; Glotzer, S. C. Self-assembly of soft-matter quasicrystals and their approximants. *Proc. Natl. Acad. Sci. U.S.A.* **2011**, *108*, 20935−20940.
(18) Jayaraman, A.; Baez-Cotto, C. M.; Mann, T. J.; Mahanthappa, M. K. Dodecagonal quasicrystals of oil-swollen ionic surfactant micelles. *Proc. Natl. Acad. Sci. U.S.A.* **2021**, *118*, No. e2101598118.
(19) Cao, Y.; Scholte, A.; Prehm, M.; Anders, C.; Chen, C.; Song, J.; Zhang, L.; He, G.; Tschierske, C.; Liu, F. Understanding the role of trapezoids in honeycomb self-assembly−pathways between a columnar liquid quasicrystal and its liquid-crystalline approximants. *Angew. Chem., Int. Ed.* **2024**, *63*, No. e202314454.
(20) Kölbel, M.; Beyersdorff, T.; Cheng, X. H.; Tschierske, C.; Kain, J.; Diele, S. Design of liquid crystalline block molecules with nonconventional mesophase morphologies: calamitic bolaamphiphiles with lateral alkyl chains. *J. Am. Chem. Soc.* **2001**, *123*, 6809−6818.
(21) Cheng, X.; Prehm, M.; Das, M. K.; Kain, J.; Baumeister, U.; Diele, S.; Leine, D.; Blume, A.; Tschierske, C. Calamitic bolaamphiphiles with (semi)perfluorinated lateral chains: polyphilic block molecules with new liquid crystalline phase structures. *J. Am. Chem. Soc.* **2003**, *125*, 10977−10996.
(22) Cheng, X.; Das, M. K.; Baumeister, U.; Diele, S.; Tschierske, C. Liquid crystalline bolaamphiphiles with semiperfluorinated lateral chains: competition between layerlike and honeycomb-like organization. *J. Am. Chem. Soc.* **2004**, *126*, 12930−12940.
(23) Cook, A. G.; Baumeister, U.; Tschierske, C. Supramolecular dendrimers: unusual mesophases of ionic liquid crystals derived from protonation of DAB dendrimers with facial amphiphilic carboxylic acids. *J. Mater. Chem.* **2005**, *15*, 1708−1721.
(24) Chen, B.; Zeng, X.; Baumeister, U.; Ungar, G.; Tschierske, C. Liquid crystalline networks composed of pentagonal, square, and triangular cylinders. *Science* **2005**, *307*, 96−99.
(25) Chen, B.; Baumeister, U.; Pelzl, G.; Das, M.; Zeng, X.; Ungar, G.; Tschierske, C. Carbohydrate rod conjugates: ternary rod-coil molecules forming complex liquid crystal structures. *J. Am. Chem. Soc.* **2005**, *127*, 16578−16591.
(26) Prehm, M.; Enders, C.; Anzahaee, M. Y.; Glettner, B.; Baumeister, U.; Tschierske, C. Distinct Columnar and Lamellar Liquid Crystalline Phases Formed by New Bolaamphiphiles with Linear and Branched Lateral Hydrocarbon Chains. *Chem. - Eur. J.* **2008**, *14*, 6352−6368.
(27) Crane, A. J.; Martinez-Veracoechea, F. J.; Escobedo, F. A.; Muller, E. A. Molecular dynamics simulation of the mesophase behaviour of a model bolaamphiphilic liquid crystal with a lateral flexible chain. *Soft Matter* **2008**, *4*, 1820−1829.
(28) Cheng, X.; Liu, F.; Zeng, X.; Ungar, G.; Kain, J.; Diele, S.; Prehm, M.; Tschierske, C. Influence of flexible spacers on liquid-crystalline self-assembly of T-shaped bolaamphiphiles. *J. Am. Chem. Soc.* **2011**, *133*, 7872−7881.
(29) Liu, X.; Yang, K.; Guo, H. Dissipative particle dynamics simulation of the phase behavior of T-shaped ternary amphiphiles possessing rodlike mesogens. *J. Phys. Chem. B* **2013**, *117*, 9106−9120.
(30) Tschierske, C.; Nürnberger, C.; Ebert, H.; Glettner, B.; Prehm, M.; Liu, F.; Zeng, X.; Ungar, G. Complex tiling patterns in liquid crystals. *Interface Focus* **2012**, *2*, 669−680.
(31) Tan, T.; Cao, Y.; Chen, C.; Ling, S.; Hou, G.; Paterson, M. J.; Wang, X.; Chen, Y.; Jiang, K.; He, G.; Ungar, G.; Mehl, G. H.; Liu, F. Tuning Aggregation in Liquid-Crystalline Squaraine Chromophores. *Adv. Sci.* **2025**, DOI: 10.1002/advs.202416249.
(32) Lifshitz, R.; Petrich, D. M. Theoretical model for Faraday waves with multiple-frequency forcing. *Phys. Rev. Lett.* **1997**, *79*, 1261.
(33) Savitz, S.; Babadi, M.; Lifshitz, R. Multiple-scale structures: from Faraday waves to soft-matter quasicrystals. *IUCrJ* **2018**, *5*, 247−268.
(34) Archer, A. J.; Ratliff, D. J.; Rucklidge, A. M.; Subramanian, P. Deriving phase field crystal theory from dynamical density functional theory: consequences of the approximations. *Phys. Rev. E* **2019**, *100*, No. 022140.
(35) Jiang, K.; Tong, J.; Zhang, P.; Shi, A.-C. Stability of two-dimensional soft quasicrystals in systems with two length scales. *Phys. Rev. E* **2015**, *92*, No. 042159.
(36) Subramanian, P.; Archer, A.; Knobloch, E.; Rucklidge, A. M. Three-dimensional icosahedral phase field quasicrystal. *Phys. Rev. Lett.* **2016**, *117*, No. 075501.
(37) Yin, J.; Jiang, K.; Shi, A.-C.; Zhang, P.; Zhang, L. Transition pathways connecting crystals and quasicrystals. *Proc. Natl. Acad. Sci. U.S.A.* **2021**, *118*, No. e2106230118.
(38) Fredrickson, G. H.; Ganesan, V.; Drolet, F. Field-theoretic computer simulation methods for polymers and complex fluids. *Macromolecules* **2002**, *35*, 16−39.
(39) Fredrickson, G. *The Equilibrium Theory of Inhomogeneous Polymers*; Oxford University Press, 2006.
(40) Shi, A.-C. *Developments in Block Copolymer Science and Technology*; John Wiley and Sons, Ltd, 2004; Chapter 8, pp 265−293.
(41) Shi, A.-C. Self-consistent field theory of inhomogeneous polymeric systems: a variational derivation. *Adv. Theory Simul.* **2019**, *2*, No. 1800188.
(42) Morse, D. C.; Fredrickson, G. H. Semiflexible polymers near interfaces. *Phys. Rev. Lett.* **1994**, *73*, 3235−3238.
(43) Gao, J.; Song, W.; Tang, P.; Yang, Y. Self-assembly of semiflexible block copolymers: 2D numerical implementation of self-consistent field theory. *Soft Matter* **2011**, *7*, 5208−5216.
(44) Jiang, Y.; Chen, J. Z. Y. Influence of chain rigidity on the phase behavior of wormlike diblock copolymers. *Phys. Rev. Lett.* **2013**, *110*, No. 138305.
(45) Liu, F.; Tang, P.; Zhang, H.; Yang, Y. Archimedean tiling patterns self-assembled from X-shaped rod-coil copolymers with hydrogen bonds. *Macromolecules* **2018**, *51*, 7807−7816.
(46) Xu, W.; Jiang, K.; Zhang, P.; Shi, A.-C. A strategy to explore stable and metastable ordered phases of block copolymers. *J. Phys. Chem. B* **2013**, *117*, 5296−5305.
(47) Stampfli, P. A dodecagonal quasiperiodic lattice in two dimensions. *Helv. Phys. Acta* **1986**, *59*, 1260−1263.
(48) Meyer, Y. *Algebraic Numbers and Harmonic Analysis*; North-Holland Publishing Company, 1972; Vol. 2.
(49) He, Z.; Jiang, K.; Tan, L.; Wang, X. High-accurate and efficient numerical algorithms for the self-consistent field theory of liquid-crystalline polymers. 2024, arxiv:2404.15363. arXiv.org e-Print archive. https://arxiv.org/abs/2404.15363.
(50) Frigo, M.; Johnson, S. G. The design and implementation of FFTW3. *Proc. IEEE* **2005**, *93*, 216−231.
(51) He, Z.; Wang, X.; Zhang, P.; Shi, A.-C.; Jiang, K. Theory of polygonal phases self-assembled from T-shaped liquid crystalline molecules. *Macromolecules* **2024**, *57*, 2154.
(52) Oxborrow, M.; Henley, C. L. Random square-triangle tilings: a model for twelvefold-symmetric quasicrystals. *Phys. Rev. B* **1993**, *48*, 6966−6998.
(53) Jansen, T.; Chapuis, G.; De Boissieu, M. *Aperiodic Crystals - from Modulated Phases to Quasicrystals*; Oxford University Press: New York, 2007; p 312.

https://doi.org/10.1021/acs.macromol.4c02380
Macromolecules 2025, 58, 5229−5239